Imaging Data From the MUSTANG Bolometer Array

W. D. Cotton, October 16, 2008

***Abstract*—Large format bolometer arrays on single dish telescopes are becoming increasingly common for imaging at millimeter and submillimeter wavelengths. This memo describes a novel approach to imaging data from a bolometer array camera. This technique is to iteratively estimate the celestial sky and background signals from the instrument, the atmosphere, etc. using a well designed observing pattern to help separate these effects in the time domain. This technique attempts the recovery of spatial structures much larger than the footprint of the array, and while imperfect, much extended structure is recoverable. This approach is applied to the MUSTANG 3 mm bolometer array on the Green Bank Telescope on both simulated data and observations of the starburst galaxy M82.**

I. Introduction

LARGE format bolometer arrays on large single dish telescopes are an efficient way of imaging at millimeter and submillimeter wavelengths and an increasing number of such instruments are either currently online or are under development (SCUBA, SHARC, BOLOCAM, GISMO...[). At these wavelengths the backgrounds are very large and variable and estimating and removing these backgrounds is one of the major difficulties in imaging data from these cameras. Imaging extended sources is especially challenging as it is difficult to separate the signals due to structures on scales larger than the footprint of the array from background variations. This memo discusses a number of these effects, especially those seen in data from the MUSTANG array [2] on the Green Bank Telescope (GBT). A method for estimating and removing these backgrounds is described and applied to data from the MUSTANG camera. An implementation of this technique in the Obit package ([1], http://www.cv.nrao.edu/∼bcotton/Obit.html) is described.

II. Background Signals

Telescope radiometers, and especially bolometers, measure the power that hits their detectors. This power comes from a number of sources in addition to that from the celestial object being observed. In addition to the background sources of power, variations in the instrument itself will cause variations in the output time stream data which mimic variations in received power. The following describes several of the major backgrounds and other sources of spurious signals and general strategies for reducing their effects.

One of the major uncontrollable sources of background is the variable emission from water vapor in the troposphere. On the largest scales, the emission varies with the airmass through which the sky is being observed; for sufficiently large fields being imaged, the variation across the field of view can be significant at any one time. For a constant, known zenith opacity, correction as a function of observing airmass is straightforward.

On smaller scales, water vapor cells have scale sizes of order a hundred meters and can introduce significant brightness variations on time scales of seconds to minutes. Since the emission is largely very close to the antenna, the lines of sight from the various detectors to the sky mostly pass through the same volume of air so this background is essentially common mode amoung the various detectors. For sources much smaller than the footprint of the array on the sky, subtracting a running median of the detector values from each data stream largely removes the atmospheric contribution. For sources which are not small compared to the footprint, it is desirable to sweep the telescope beams over the source at a sufficiently high speed that the modulation of the celestial signals is faster than the variation of the atmospheric signals.

Most wideband detectors suffer from "1/f" noise at some level; this is caused by low level gain fluctuations whose power spectrum is "red" meaning larger fluctuations on longer timescales. Removal of this background is also helped by a rapid motion of the telescope beams over the sky to help separate the instrumental from the celestial signals in the time domain. Repeated, frequent reobservation of the same position of the sky also helps constrain this background.

Other instrumental variations can also modulate the bolometer detector outputs in ways which may-or-may-not equally effect all detectors. One such common mode signal is the 1.4 Hz variations from the pulse tube refrigerator on the MUSTANG array.

III. MUSTANG Array

MUSTANG (Multiplexed SQUID TES array at Ninety GHz) [2] is a 64 element bolometer array operating at 90 GHz on the Green Bank Telescope (GBT) giving about 8" resolution. MUSTANG was commissioned during the winters of 2006–2007 and 2007–2008 and has begun preliminary science operations.

A. Observing Patterns

The instrument observes by scanning rapidly over the field to be imaged with the bolometer data streams sampled at a constant, 1 kHz rate. The current observation modes are "daisy" and "boxscan" patterns; both are continious scanning patterns. The former makes repeated passes through the center

National Radio Astronomy Observatory, 520 Edgemont Rd., Charlottesville, VA, 22903 USA email: bcotton@nrao.edu

Manuscript received ; revised

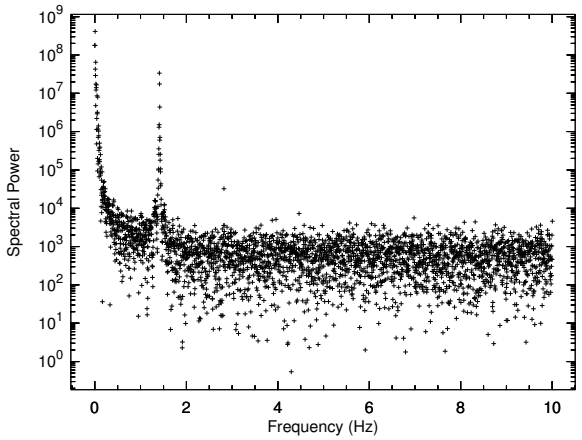

Fig. 1. The power spectrum of a segment of output data from one element of the MUSTANG array on the GBT. The sharp increase towards the lowest frequencies is characteristic of both the atmospheric and "1/f" noise contributions. The 1.4 Hz modulation due to the pulse tube cooler is also prominent.

of a circular scan region and the latter uniformly covers a rectangular regions with a pattern of nearly orthoginal passes.

B. Calibration

Amplitude and gain calibration is performed using an internal calibration source that is cycled between the "on" and "off" states. The data are calibrated by comparing the response to this calibration source to that of a planet of known brightness. Partial daisy patterns on bright quasars are used for focus and pointing measurements. Focus corrections are applied during the observations but pointing corrections are applied off–line. Currently a constant zenith opacity of 10% is used. The weather in Green Bank is seldom better than this; if it is much worse than this, the data is of questionable use.

C. Correction of Internal Oscillations

The MUSTANG bolometer detectors are very sensitive detectors of power in any form and are sensitive to mechanical power from the pulse tube cooling mechanism. This introduces a very narrow band modulation of the detector outputs from all detectors; an example power spectrum is shown in Figure 1. Since this is a very strong signal, it is easily estimated and removed from the time–stream data. A simple notch filter approach is inappropriate as this will also remove power from the sky signal at this frequency introducing artifacts. This is especially the case when there are strong gradients in the sky brightness such as around bright point sources. It was empirically determined that this signal has a very narrow intrinsic width and is centered near 1.41170 Hz. A sine wave at this frequency with common phase and detector dependent amplitude was fitted to, and removed from, the detector timestream data for each scan. A sample of data before and after this filtering is shown in Figure 2.

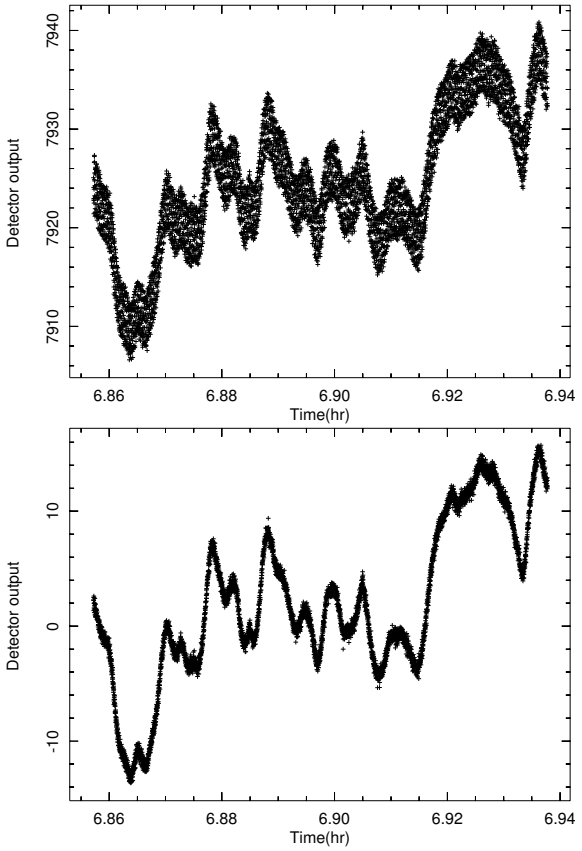

Fig. 2. The upper plot shows the time sequence of 5 minutes of 20 Hz averaged data from a single MUSTANG detector including the 1.4 Hz signal as a function of time. The lower plot shows the same data after fitting and subtracting the 1.4 Hz signal.

IV. On the Fly Imaging

In the "On-the-Fly" (OTF) imaging technique, the telescope is swept across the field of view in a pattern that will cover all of the field to be imaged while sampling data at a constant rate. The data sampling should be fast compared the the time it takes the beam to move its own width or the sky will be smeared out. In this mode, the sky is sampled at uniform times but at positions not constrained to the pixels on a well defined grid. As this is the case, the actual position on the sky of each detector must be accurately known at all times.

The conversion of the "randomly" sampled data to a regular grid proceeds in a number of steps collectively called "griding".

1) "Convolution" and re-sampling on a grid
   Each sample is considered as a delta function and is multiplied by a continuous "griding" (AKA "convolution") function. The gridding function is centered on the datum and is sampled on a grid centered on the pixel nearest to the datum and which is of finite support. This results in a grid of data*griding_function as well as a grid of griding_function values.
2) Accumulation onto a grid
   The data times the griding function and the griding function samples are accumulated onto a pair of grids covering the region of the sky to be imaged.
3) Normalization
   When all of the data have been multiplied by the griding function, re sampled and accumulated onto the grids, the image is normalized by dividing the sum

of the data*griding_function grid by the sum of the griding_function grid on a pixel-by-pixel basis.

In general, not all data are of the same quality, e.g. varying sensitivity among detectors, and each datum may be assigned a statistical weight. These weights are included in the process described above by replacing the griding function with the product of the griding function times the weight of the datum being gridded.

In the griding procedure, the griding function plays a critical role and the function chosen is generally a compromise. One of the compromises is sensitivity against resolution. Using a "fatter" griding function will include more data in each pixel and thus give lower noise at the cost of reduced resolution. The implementation in Obit provides a number of gridding functions but the exponential$\times$sinc sees a good compromise.

The resolution of the derived image affects the units which, by convention, are expressed in Jansky per beam area. Any operation that modifies the resolution (beam area) must be reflected in the units of the derived image. In general, this requires a scaling by the ratio of the beam areas.

V. Iterative Background Estimation

In the following discussion the contributions to the detector outputs are considered to be of two types; 1) response to the celestial sky which we desire to estimate and 2) "backgrounds" which are everything else.

A. Overview

The principle difficulty with imaging short wavelength radio continuum single dish data is the large and variable background signal. This background comes from the atmosphere, the telescope and the instrument itself and can vary on a wide variety of timescales. The offset of the measured signals from zero is particularly difficult to obtain and generally must be determined from some knowledge of the (astronomically interesting) sky. The basic approach described here is to iteratively model the background signals, image the sky, subtract a model of the astronomical sky from the data and reestimate the backgrounds. The estimate of the background is determined from the residual data (sky model subtracted) by a low pass filtering. As the quality of the model improves, higher temporal frequency components of the residuals are included.

This technique uses the redundancy in the data to separate the constant astronomical sky from the variable background signals. The zero level is set essentially by the constraint that the sky brightness in some regions imaged are zero or otherwise known. This technique works best if the telescope beams can be swept over the field of view sufficiently rapidly that the modulation of the signal due to the astronomical sky is faster than the time scale of the variations of the background signals.

The redundancy in the data are of two forms. The first is that each resolution element in the image is covered multiple times by the instrument, preferably along different trajectories on the sky as in the "basket–weaving" technique.

For instruments with multiple pixels, such as the MUSTANG bolometer array, there is additional information. The contributions of the atmosphere will be essentially the same in all detectors, i.e. a common mode signal, as the various beams strongly overlap through the regions of the atmosphere in which the bulk of the variations in emission occur. In the case of MUSTANG, much of the background variation from the instrument itself (e.g. the 1.4 Hz variations due to the refrigerator pump) are also common mode. For sources smaller than the detector array, these common mode backgrounds are easily distinguished from the source signals which appear in only a few pixels. Any prior knowledge of the sky (e.g areas with no emission) can be introduced as constraints on the sky model.

B. CLEAN as Sky Model

In order to use the method outlined above, a sky model must be derived from the image obtained from the data. The use of a griding function in the image formation in general has a point spread function (psf) different from the intrinsic resolution of the telescope so this image is not directly useable In addition, there may be artifacts in the image resulting from imperfect background estimation that should not be included in the sky model.

One form of sky model is that obtained from a CLEAN deconvolution of the image derived from the data. CLEAN effectively decomposes an image into a set of delta function which can then be restored using a well behaved approximation of the telescope psf. The telescope response to this sky model can then be determined from a simple interpolation of the CLEAN restored image. In addition, CLEAN windowing can be used to constrain the region in which emission is allowed. For the CLEAN sky model, the residuals are not included which gives the region outside of the CLEAN window zero flux density. Additional constraints such as positivity can also be imposed on the sky model as appropriate.

If the CLEAN sky model is derived from an image with resolution different from the telescope, the units of the sky model image must be scaled to those appropriate for the telescope data. Such resolution changes are inherent in the OTF imaging process.

C. Extended Emission

There is a fundamental degeneracy between celestial structures larger than the footprint of the array on the sky and the background signals. This degeneracy can be partially alleviated by very rapid motions of the telescope to modulate the sky signal faster than the backgrounds are varying and separate the effects in the time domain. This process can be greatly assisted if even imperfect knowledge of the sky brightness model can be used. Using the iterative background estimation technique, sky models derived removing only slow background variations are used to prevent large scale structure from being absorbed into the backgrounds estimated on shorter timescales.

In principle, this technique can be applied to a larger scale of iteration and repeating the entire sequence of background estimation by starting the process with the final sky model of a previous processing. Excessive use of this technique has its difficulties as well as it is possible to invent spurious

large scale structure as well as remove it. Experience suggests a single reprocessing starting with the previous model help recover most of the extended emission (largely eliminates the bowls around large sources) but the effects of further iteration have not been explored.

D. Residual Calibration

Residual calibration consists of a number of steps allowing the detector outputs to be converted into Jy., data weights to be estimated, and the background signal levels estimated. The process described here is specific to MUSTANG but could be adapted for other, similar instruments.

1) Subtraction of Sky Model: The CLEAN process reduces the image of the sky to a set of delta functions. The response of the telescope to this model of the sky is given by the convolution of this set of delta functions with the telescope psf. Note: in general this is different from the psf of the "dirty" image subjected to the CLEAN. The CLEAN delta functions after convolution with the instrumental psf and scaling into the appropriate units, can have any additional physical constraints imposed (e.g. positivity) and used to derive the instrumental response to the sky model by simple interpolation. To produce a residual data set, the instrumental response to the model is evaluated at the position in the sky model of all data samples and subtracted from those samples.

2) Backgrounds from filtered residuals: To the degree that the sky model is a perfect representation of both the true sky and the telescope psf, the residual data should contain only the background signals and the time series representing the backgrounds can be derived from a filtering of the residual data. Since the data sampling rate is significantly faster than variations in either the response to the sky and variations in the background, this filtering should be a low pass filter. Early in the iteration, the sky model will be imperfect and the filtering should pass only temporal frequencies in the residual data long compared to the time it takes the telescope beam to pass over structures in the sky. Then, as the sky model improves, higher temporal frequencies can be included in the estimated background.

3) Common mode vs. detector backgrounds: Background signals come from a number of different causes, those associated with individual detectors (e.g. gain variations) will be largely independent from detector to detector. Those backgrounds which are common to all detectors (e.g. tropospheric emission) will have approximately equal effects on all detectors and can be considered common mode effects. The detector specific and common mode effects may occur on different timescales and can be determined separately.

E. Iterative Background Estimation Process

The outline of the background estimation algorithm is shown in Figure 3. After an initial set of calibrations based on external measurements, an iterative refinement of the sky model and the backgrounds is performed on the data themselves. As the accuracy of the sky model improves from cycle to cycle, the filter timescale (τ) is reduced until it approaches that of the actual background; for the MUSTANG array this is usually of the order of one second as can be seen in Figure 1. Since the detectors themselves exhibit variations, the background estimated switches between that of individual detectors and the common mode background. Timescales for estimation of detector offsets are longer than for common mode backgrounds. Following are explanations of the boxes in Figure 3.

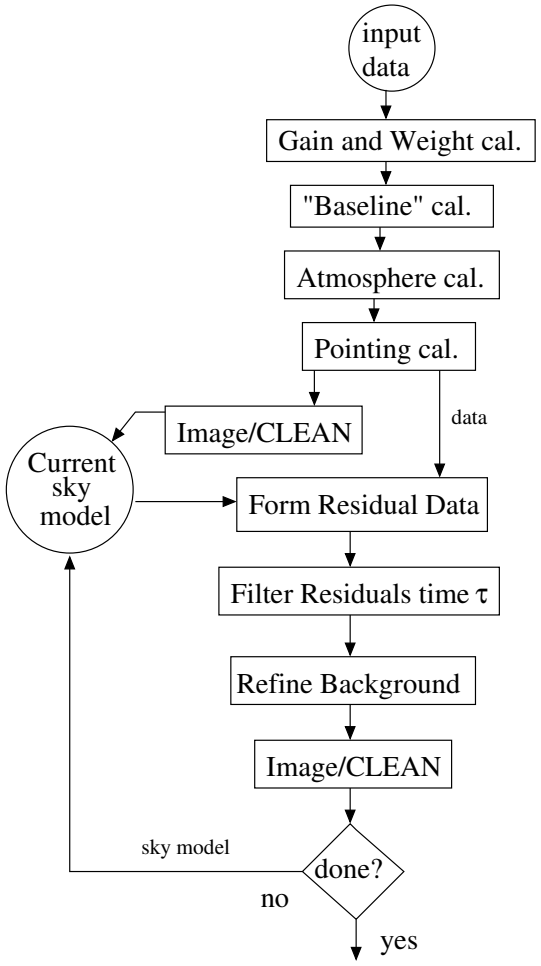

Fig. 3. Flow diagram of the iterative background estimation process. Each iteration the timescale, τ, of the filtering is reduced. Background type can alternate between common mode and detector. See the text for an explanation of each box.

- **Gain and Weight Calibration**
  The gain of each detector is determined from scans with a cyclic firing of the MUSTANG internal calibration source. The equivalent source strength in Jy is determined by comparing the strength of the response to the internal calibration source to that of a strong source (planet) of known brightness. The strength of the calibration source is determined by subtracting the average "Cal-off" signal prior to and following the "Cal-on" signal. This signal is used to both stabilize the detector gains and convert the signal strengths into Janskys. Not all detectors are equally sensitive and the relative weights are determined from the RMS fluctuations in short scans of blank sky measurements.

- **"Baseline" calibration**
  The "baseline" for each detector in each scan is estimated using a low pass filter on the data. The time scale from this filtering needs to be long enough not to remove significant power from any astronomical signals.
- **Atmospheric calibration**
  For multi-beam systems such as MUSTANG, the atmospheric contributions to the background are expected to be largely common among all the detectors. After the application of the previous calibration, a single offset for each detector and a piecewise linear common mode atmospheric offset series in time is robustly estimated. The timescale of the linear common mode segments is sufficiently long not to significantly impact the astronomical portion of the signal. Gain corrections are also made for the estimated zenith opacity and the airmass of each data sample.
- **Pointing calibration**
  Corrections to the telescope pointing are made by linear interpolation of the pointing errors in azimuth and elevation as determined from the focus/pointing scans on nearby calibrator sources.
- **Image/CLEAN**
  After application of the best available calibration, the data are imaged as described in section IV and a sky model formed using CLEAN as described in section V-B. This sky model image has the psf of the telescope.
- **Form Residual Data**
  The sky model is interpolated to the position of each data sample and subtracted from the calibrated dataset to produce a residual dataset.
- **Filter Residuals**
  The residual data set is subjected to a low–pass time filter to remove timescales shorter than a time constant τ.
- **Refine Background**
  The filtered residual data are resampled to produce a refined estimate of the time variable background. This background estimate can be either per detector or a common mode estimated from the median detector value. The timescale τ used for detector offsets is longer than that used for common mode background.

VI. Examples

The following sections give examples of applying the iterative background estimation technique to both a set of simulated sources (with real backgrounds) as well as actual observations with the MUSTANG array on the GBT.

A. Simulated Sky, Real Backgrounds

Imaging simulated data has the advantage of knowing the "Ground Truth" and provides an oportunity to test the ability of this technique to recover structures on size scales larger than the foot print of the detector on the sky. While simulating the sky is straightforward, simulating realistic backgrounds is not. For this purpose, we will use actual observations of a blank portion of the sky obtained with MUSTANG on the GBT and add point and Gaussian components to the data after the initial calibration steps and prior to the first imaging in Figure 3. The image derived from this data has an RMS nise of 1.9 mJy/beam For this purpose, the psf of the GBT was taken to be an 8" FWHM Gaussian.

TABLE I
Model 1 Parameters

x pixel	y pixel	Flux Jy	Maj FWHM "	Min FWHM "	PA °
117.50	115.75	0.07	8.0	8.0	
127.50	152.33	0.05	8.0	8.0	
129.00	129.00	0.40	16.0	16.0	
137.75	117.25	0.30	80.0	8.0	160.0

Fitted Parameters

x pixel	y pixel	Flux Jy	Maj FWHM "	Min FWHM "	PA °
117.51	115.73	0.0653	8.3	7.7	0.0
127.47	152.28	0.0480	8.3	7.7	33.4
129.01	129.03	0.307	14.5	13.9	-132.2
136.44	113.70	0.246	83.4	7.0	160.1

1) Single Point Source Model: The first test is one in which a single point source (convolved to the 8" GBT psf) was added to the set of blank sky observations. The data were subjected to four sets of iterations of the loop in Figure 3 with minimum timescales (τ) of 6, 3, 1 and 1 times one second. Each of these consisted of an detector specific estimation with timescales three times τ followed by a common mode background estimation with timescale τ. Imaging used the default exponential$\times$sinc gridding function which increases the resolution of the image to 7.5". CLEAN was allowed to locate components in all but the high noise, outer regions of the image. A Gaussian fitted to the derived (Dirty) image gives a location within 0.02" of the correct location, a size of 7.75"$\times$7.43" and an integrated flux density of 0.095 Jy whereas the input model has 0.1 Jy. the resultant image is shown with the model in Figure 4.

2) Extended Source Model 1: Next a more complex model was used which contains both point sources and a source with extent significantly larger than the array foot print on one axis. The model parameters are given in Table I. The simulated data were processed as in the previous example; the resultant image is shown with the model in Figure 5 and the parameters of the Gaussians fitted to the images are given in Table I

3) Extended Source Model 2: An even more complex model was then used which contains both point sources and sources with sizes significantly larger than the array foot print on one or both axes. The model parameters are given in Table II. The simulated data were processed as in the previous examples; the resultant image is shown with the model in Figure 6 and the parameters of the Gaussians fitted to the images are given in Table II

4) Extended Source Model 3: Finally model which contains both point sources and a very large source. The model parameters are given in Table III. The simulated data were

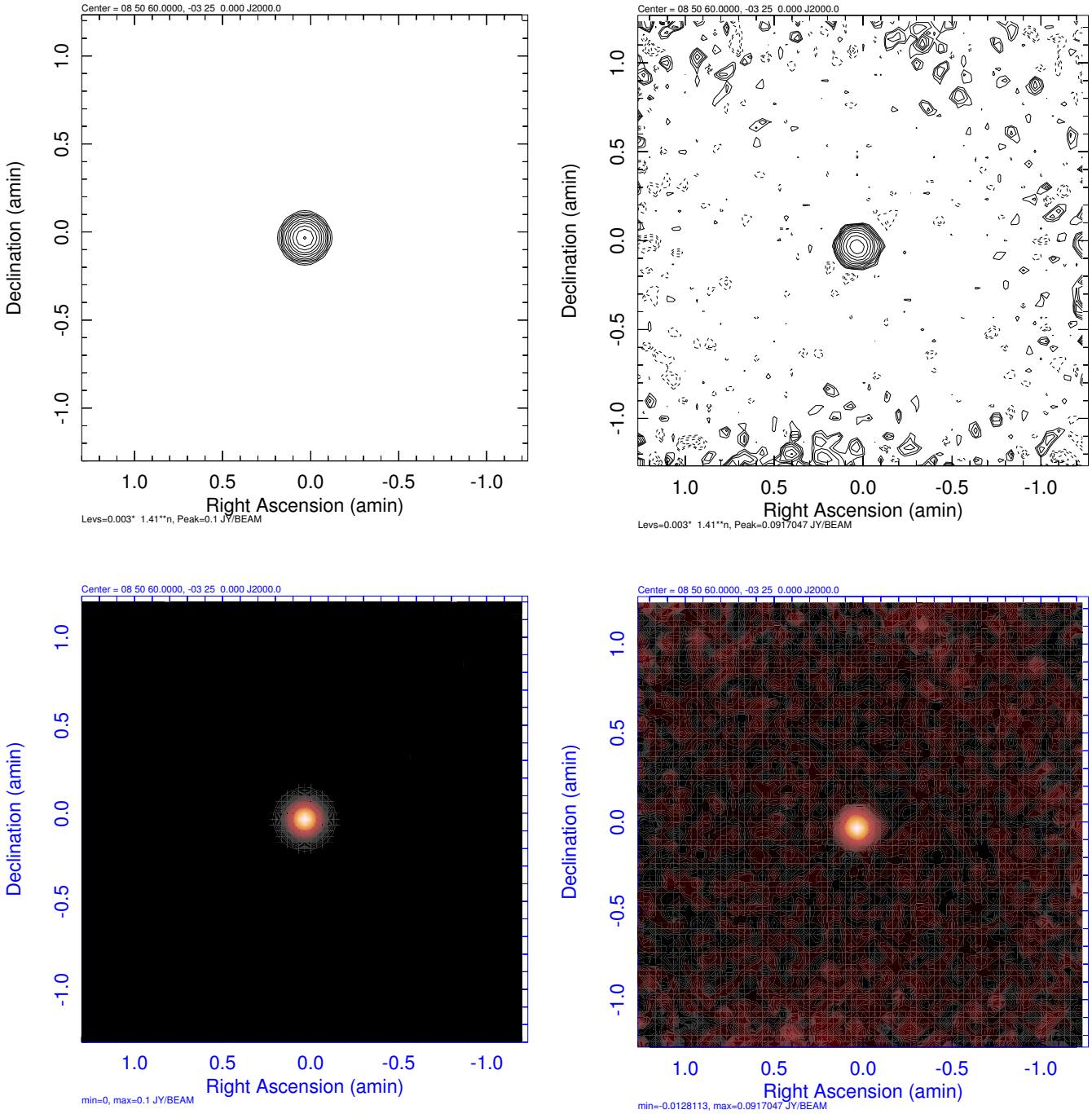

Fig. 4. Point Model: Simulated sky with real backgrounds. On the left is the model and the right the reconstructed image; on the top are contour plots and the bottom pseudo color images. Both contour have the same levels which are powers of $\sqrt{2}$. The increase in noise towards the edge of the plot on the right is a result of the variable coverage of the blank sky observations used for the simulation.

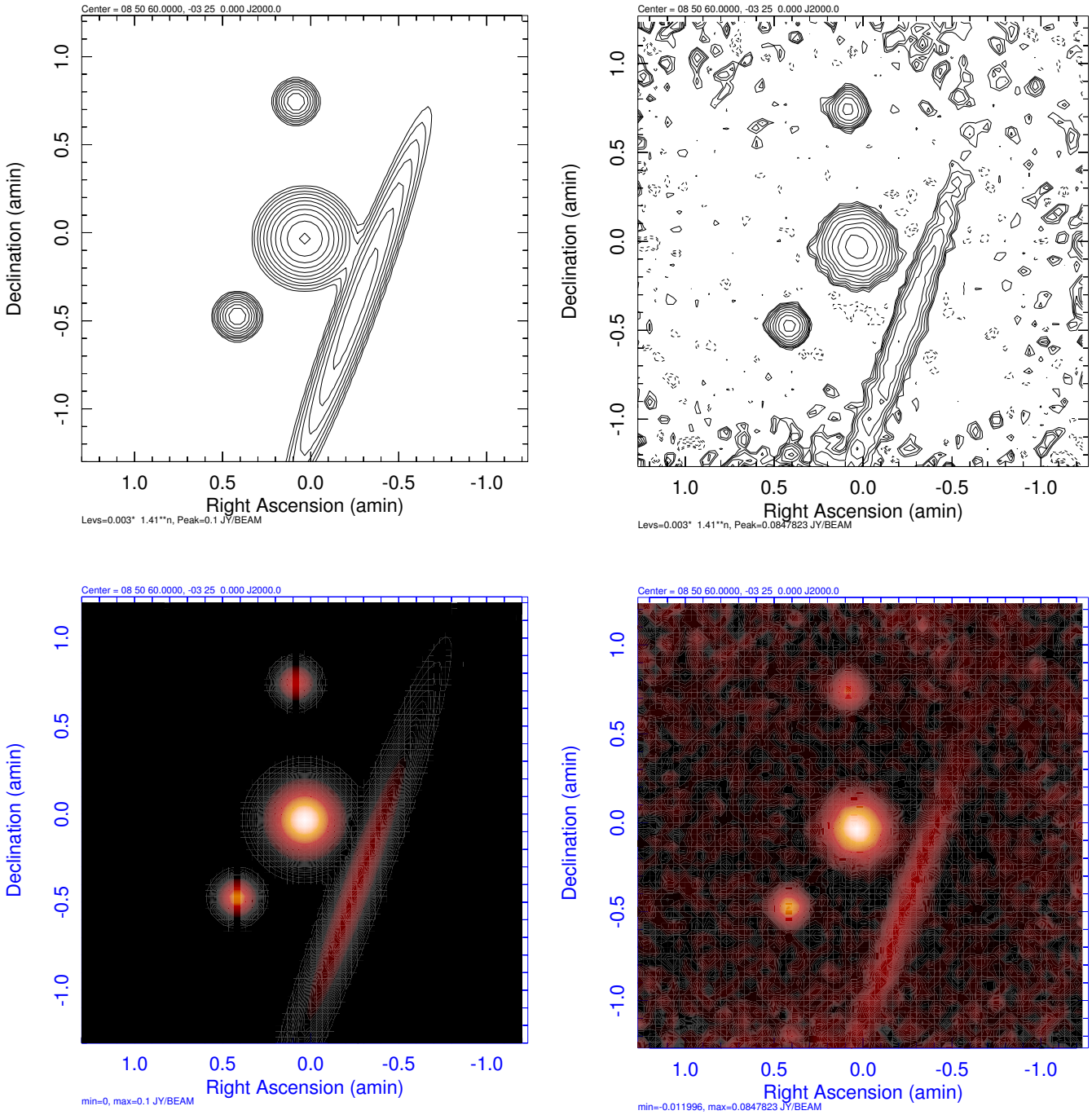

Fig. 5. Extended Model 1: Simulated sky with real backgrounds. On the left is the model and the right the reconstructed image; on the top are contour plots and the bottom pseudo color images. Both contour plots have the same levels which are powers of $\sqrt{2}$.

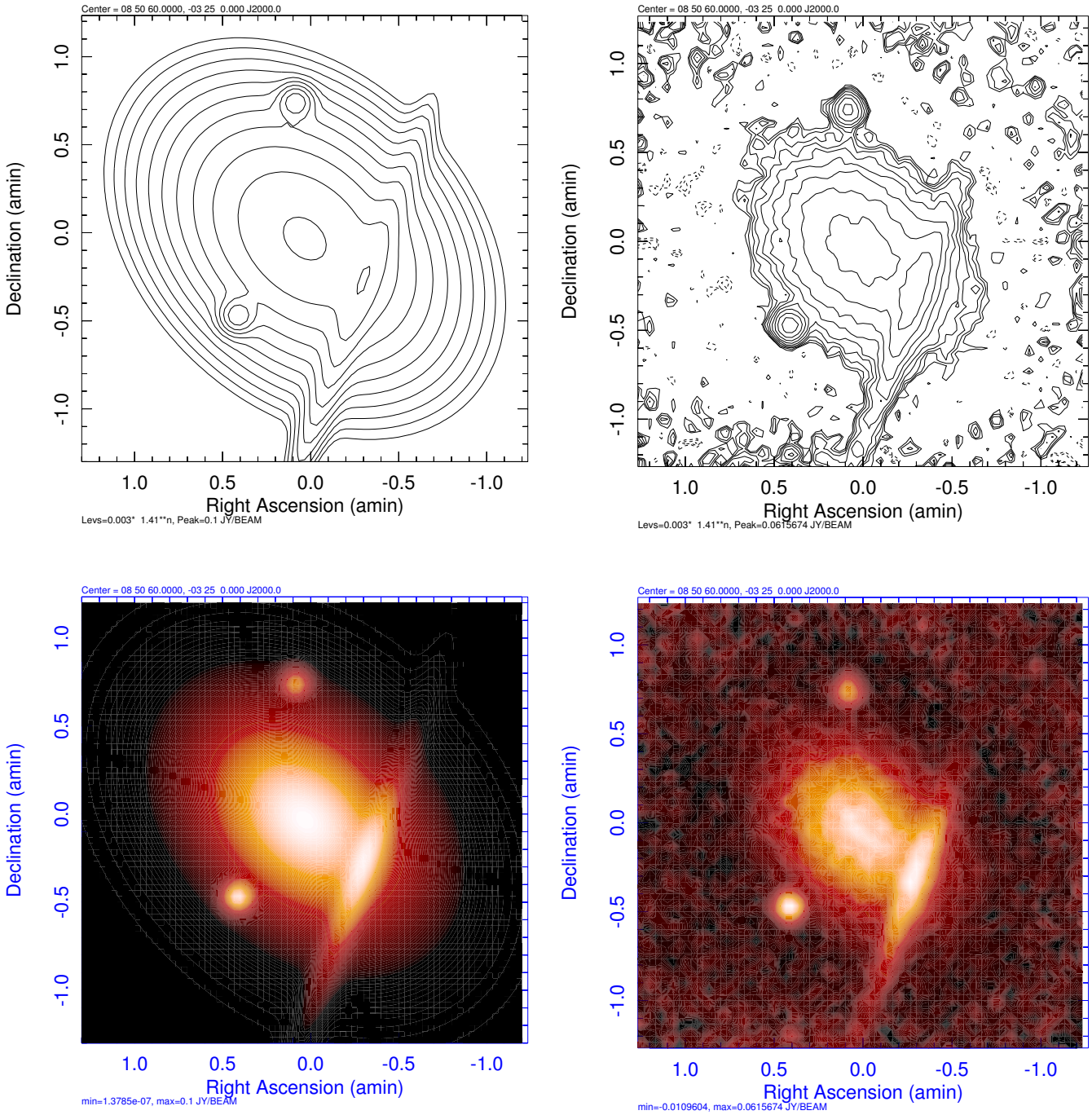

Fig. 6. Extended Model 2: Simulated sky with real backgrounds. On the left is the model and the right the reconstructed image; on the top are contour plots and the bottom pseudo color images. Both contour plots have the same levels which are powers of $\sqrt{2}$.

TABLE II
MODEL PARAMETERS

x pixel	y pixel	Flux Jy	Maj FWHM ”	Min FWHM ”	PA °
117.50	115.75	0.07	8.0	8.0	
127.50	152.33	0.05	8.0	8.0	
129.00	129.00	5.47	70.0	50.0	-135.0
137.75	117.25	0.30	80.0	8.0	160.0

Fitted Parameters

x pixel	y pixel	Flux Jy	Maj FWHM ”	Min FWHM ”	PA °
117.54	115.77	0.0652	7.9	7.1	2.6
127.49	152.25	0.0409	7.7	7.6	180.6
129.35	128.64	1.870	49.5	36.1	-136.7
138.10	117.48	0.299	62.8	8.4	160.3

TABLE III
MODEL 3 PARAMETERS

x pixel	y pixel	Flux Jy	Maj FWHM ”	Min FWHM ”	PA °
117.50	115.75	0.07	8.0	8.0	
127.50	152.33	0.05	8.0	8.0	
129.00	129.00	9.38	100.0	60.0	135.0

Fitted Parameters

x pixel	y pixel	Flux Jy	Maj FWHM ”	Min FWHM ”	PA °
117.48	115.76	0.0694	8.0	7.7	-141.8
127.56	152.22	0.0400	7.7	7.0	89.1
129.75	129.00	2.94	77.1	41.0	137.4

processed as in the previous example; the resultant image is shown with the model in Figure 7 and the parameters of the Gaussians fitted to the images are given in Table III

As can be seen in Figures 4–7 and Tables I–III, the basic features of the input models are recovered, even structure which is much larger then the footprint of the array on the sky. The locations of the reconstructed components are very close to the model values as are the axial ratios and orientations of the extended components. However, the reconstructions are imperfect, the reconstructed flux densities of the components are lower than the model value, especially so for the most extended and weakest components. The dimensions of components which are much larger than the footprint of the array are about 75% of the model values.

B. Starburst galaxy M82

An example application of this technique on real sky data is imaging of observations of the nearby starburst galaxy M82. These observations were made on 2008 March 24 using the MUSTANG array on the GBT and were processed in a fashion similar to the simulated data tests. The resultant image is shown in Figure 8. These observations consisted of 55.2 minutes of on sky integration using a mix of boxscan and daisy patterns on 3 pointing centers. The RMS in the central part of the image is 4.5 mJy/beam and the total CLEAN flux density in the image is 1.54 Jy. The only emission detected is from the strong starburst area in the very center of this galaxy.

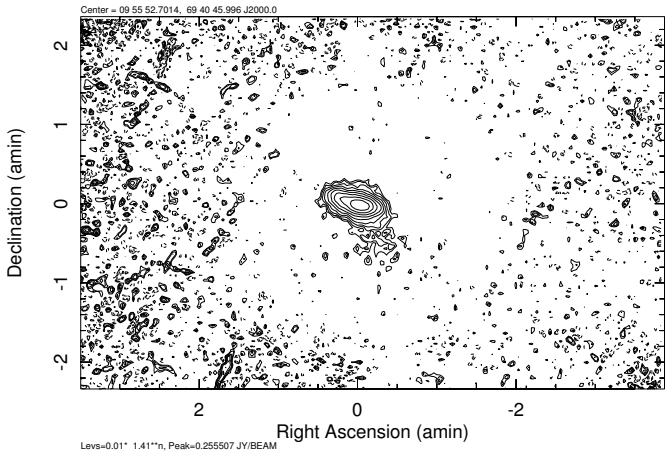

Fig. 8. Central region of the starburst galaxy M82. Contours are powers of $\sqrt{2}$ above 0.01 Jy/Beam. The increase in noise towards the edge image are due to decreasing integration times.

VII. CONCLUSIONS

The iterative background technique presented above appears to do a good job of estimating and removing background signals from observations taken with the MUSTANG array on the GBT telescope. Tests using simulated data with observed background signals show that the process can recover most of the emission from sources smaller than the footprint of the array on the sky as well as a substantial fraction of the emission from features considerably larger than the array footprint. Observations with the MUSTANG array on the GBT of the nearby starburst galaxy M82 are presented. These observations only show detectable emission in the region of strong star forming activiry in the very center of the galaxy.

REFERENCES

[1] W. D. Cotton, “Obit: A Development Environment for Astronomical Algorithms,” *PASP*, vol. 120, pp. 439–448, 2008.

[2] B. Mason, S. Dicker, P. Korngut, D. Benford, J. Chervenak, M. Devlin, E. Figueroa, J. Forgione, K. Irwin, M. Mello, S. Maher, H. Moseley, R. Norrod, J. Staghun, and S. White, “First Light with MUSTANG: A 90 GHz Bolometer Array for the Green Bank Telescope,” in *Frontiers of Astrophysics: A Celebration of NRAO’s 50th Anniversary*, ser. Astronomical Society of the Pacific Conference Series, A. H. Bridle, J. J. Condon, and G. C. Hunt, Eds., vol. 395, Aug. 2008, pp. 374–+.

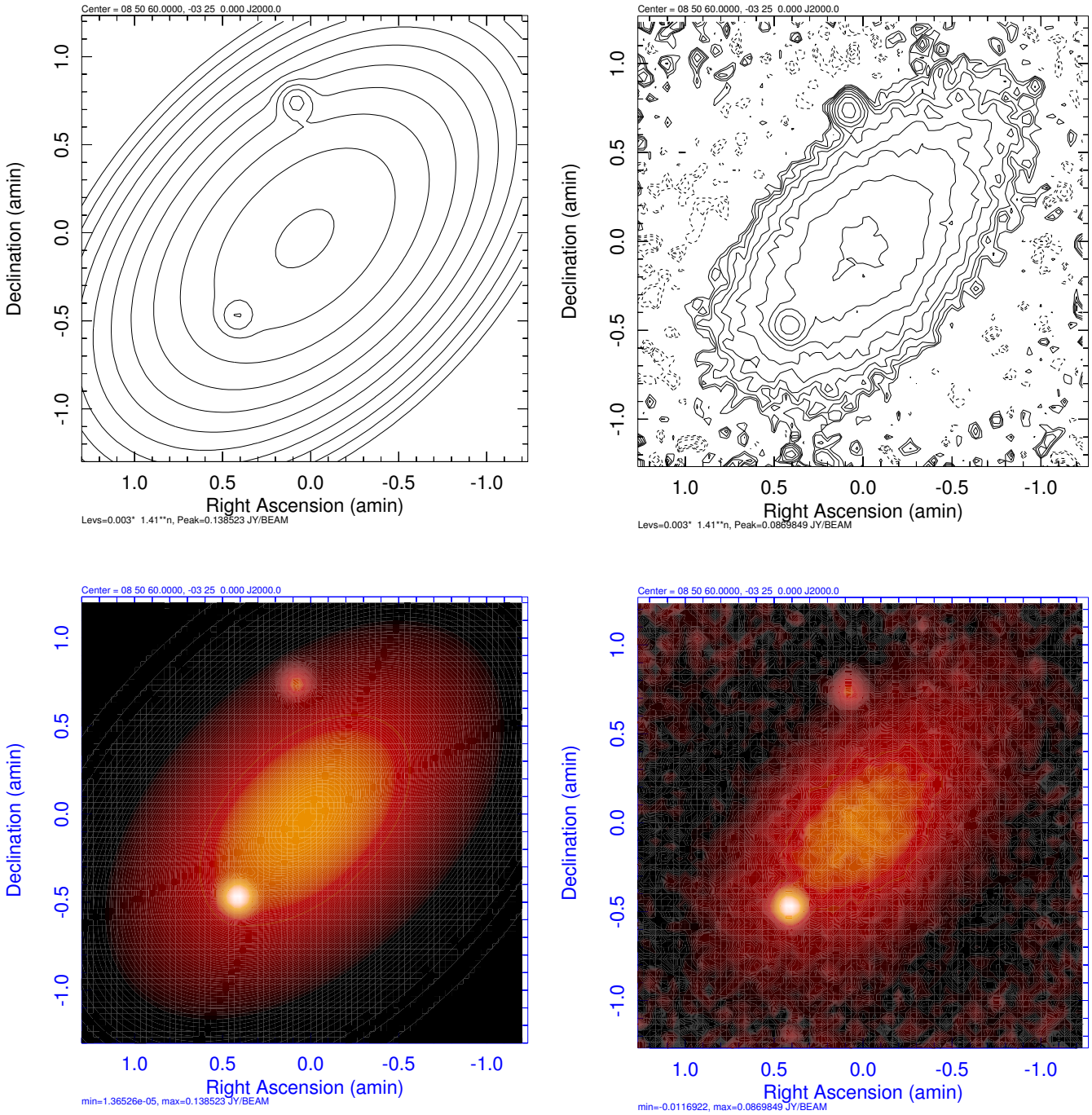

Fig. 7. Extended Model 3: Simulated sky with real backgrounds. On the left is the model and the right the reconstructed image; on the top are contour plots and the bottom pseudo color images. Both contour plots have the same levels which are powers of $\sqrt{2}$.